ChemElectroChem

Research Article
doi.org/10.1002/celc.202201129

Chemistry Europe
European Chemical Societies Publishing

www.chemelectrochem.org

Special Collection

Green Synthesis of Carbon Nanospheres for Enhanced Electrochemical Sensing of Dopamine

Peng Lei,[a, b] Ying Zhou,[a] Xincheng Sun,[a] Chuan Dong,[a] Yinghe He,[b] Yang Liu,*[b] and Shaomin Shuang*[a]

The detection of dopamine (DA) has received enormous attention since it is widely recognized as an important neurotransmitter associated with nerve signaling and some diseases. In this work, glucose-derived carbon nanospheres (CNs) are synthesized by the green hydrothermal approach and are served to modify electrodes for the detection of DA. The CNs were successfully synthesized and were investigated in detail by various characterization technologies. The CNs modified glassy carbon electrode (CNs/GCE) exhibits better electrochemical sensing performance with a wide linear range of 0.05–1600 μM and a low limit of 8.3 nM for determination of DA, as compared with the modified electrodes reported previously. The CNs/GCE was successfully applied to detect DA in human serum samples, which makes it promising for a variety of biomedical applications. More importantly, this work shows a novel green and simple strategy for the development of cost-effective and high-performance sensing materials, which provides more opportunities for design of electrochemical sensors with future capabilities of mass production in practical applications.

Introduction

Dopamine (DA) is an essential catecholamine neurotransmitter and plays a significant role in regulating various physiological functions of the central nervous system.[1] The content of DA is the highest (50 nmol g^{-1}) in the caudate nucleus of the human brain.[2] However, the abnormal concentration of DA is closely related to neurological and physiological diseases, particularly Parkinson's disease.[3,4] Since DA is the main neurotransmitter used for disease diagnosis, the detection of DA *in vivo* and *in vitro* is of clinical significance. A variety of biosensing methods, such as flow-injection analysis,[5] fluorescence spectrophotometry,[6] and capillary electrophoresis,[7] have been successfully employed for the determination of DA. However, the application of these methods is limited by the complicated operation processes, insufficient anti-interference ability, and high cost.[8,9] The electrochemical analysis method has attracted more and more attention owing to its advantages of easy operation, low specific investment cost, and high sensitivity.[10] Therefore, the development of green, non-toxic, high catalytic electrochemical sensing materials are especially critical.

The application of nanomaterials in electrochemical sensing has opened up a new path to better understanding the redox process for the detection of analytes through the electrochemical method. Carbon nanomaterials, including multi-walled carbon nanotubes,[11] graphene,[12] carbon nanorods,[13] fullerenes,[14] and carbon nanospheres (CNs),[15] have aroused extensive attention due to their outstanding electrochemical performance. Among these nanomaterials, CNs have played crucial roles in imaging,[16] water splitting,[17] supercapacitors,[18] and electrochemical sensing[19] owing to their ordered structures, excellent mechanical stability, and easy dispersion.[20] For example, Zhang and co – workers designed hollow CNs dotted with Gd–Fe nanoparticles to achieve magnetic resonance and photoacoustic imaging *in vivo*.[16] Li et al. prepared Co–Mo–P CNs derived from metal-organic frameworks as a high-performance electrocatalyst towards efficient water splitting, which exhibited excellent electrocatalytic performance.[17] Ultrasmall CNs with tailored sizes and textural properties were designed by the miniemulsion polymerization technique, which demonstrated excellent supercapacitive performances.[18] Pd nanoparticles decorated N-doped graphene quantum dots@N-doped hollow CNs with high electrochemical sensing performance were constructed for the ultrasensitive and highly specific detection of H_2O_2 secreted from living cancer cells.[19]

Although CN-based materials have been used in many fields previously, in this paper, the CNs synthesized by a hydrothermal method using glucose as a carbon source were employed for electrochemical sensing of DA for the first time (Scheme 1). The glucose-derived CNs offer many benefits as electrode modification materials including (a) the high hydrophilicity and good biocompatibility due to a large number of hydroxyl groups; (b) the completely non-toxic and green preparation process; (c) the

[a] Dr. P. Lei, Dr. Y. Zhou, Dr. X. Sun, Prof. Dr. C. Dong, Prof. Dr. S. Shuang
School of Chemistry and Chemical Engineering and Institute of Environmental Science
Shanxi University
Taiyuan 030006 (China)
E-mail: smshuang@sxu.edu.cn
[b] Dr. P. Lei, Prof. Dr. Y. He, Dr. Y. Liu
College of Science and Engineering
James Cook University
Queensland 4811 (Australia)
E-mail: yang.liu11@jcu.edu.au

Supporting information for this article is available on the WWW under https://doi.org/10.1002/celc.202201129

Special Collection An invited contribution to the Early Career Women in Electrochemistry Special Collection

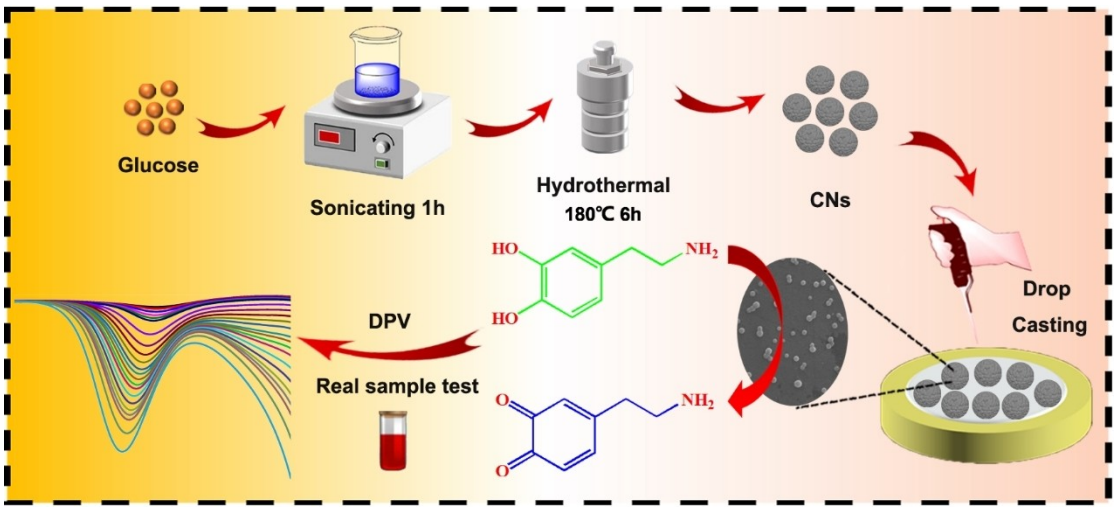

Scheme 1. Schematic illustration for the preparation of the CNs, and the fabrication and detection process of CNs/GCE.

large electroactive area and facile electron transfer kinetics for enhancing electrochemical sensitivity. The experimental results showed that the proposed sensor achieved a wider linear range with a lower detection limit for the detection of DA as compared with the DA sensors reported previously. In addition, satisfactory results were obtained when the CNs/GCE was applied to determine DA in serum, demonstrating the practical applicability of the proposed analytical method.

Results and Discussion

Physico-chemical characterization of the CNs

The XRD pattern obtained from the powdered forms of the CNs was depicted in Figure 1A. The XRD pattern showed two peaks at 20.5° and 40.3°, which can be assigned to the [002] and [100] planes of the carbon material.[21] The characteristic Fourier Transform Infrared (FTIR) bands of the CNs at 1703 cm^{-1} and 1612 cm^{-1} in Figure 1B were assigned to C=O and C=C groups, respectively.[22] The bands in the range from 1000 cm^{-1} to 1300 cm^{-1} for C–OH stretching and OH bending vibrations implied the existence of numerous residual hydroxyl groups, which can improve the hydrophilicity and the biocompatibility of the CNs. To evaluate the biocompatibility of the CNs, PC12 cells were co-cultured with various concentrations of the CNs. As shown in the MTT assay (Figure S3), the normal PC12 cells retained the viability of more than 95% even when the concentration of CNs reached 200 μg/mL, indicating that CNs had good biocompatibility and very low toxicity to normal cells. The porosity of the CNs was evaluated by nitrogen adsorption – desorption measurement. Figure 1C shows a type-IV isotherm with a hysteresis loop behavior, indicating the mesoporous nature of the CNs. The obtained BET surface area of the CNs was 58.6 $m^2 g^{-1}$ with a total pore volume of 0.30 $cm^3 g^{-1}$. The mean particle size of the CNs was found to be 200 nm, measured by the DLS system. (Figure 1D). The zeta potential of the CN was -41.3 ± 2.01 mV in an aqueous solution (Figure 1E).

Figure 2 shows the XPS spectra for the CNs over a wide binding energy range, demonstrating that the CNs are composed of C 1s and O 1s. In the C 1s spectra (Figure 2B), the peaks observed at 284.7 eV, 285.9 eV, and 288.4 eV can be attributed to C–C, C=C, and C=O, respectively.[23] Figure 2C shows the high-resolution XPS spectra of O 1s, which includes two peaks at 532.2 eV and 533.1 eV, corresponding to C–OH and C=O, respectively. The UV–visible absorption spectra of the CNs exhibited a wide characteristic peak at 348 nm (Figure S1). The morphological features of the CNs were characterized by FESEM and TEM, demonstrating that the CNs are spherical and are highly monodispersed with distinct shape boundaries (Figure 2D and 2E). The diameter of the CNs were observed to be 50–100 nm, which was smaller than the value obtained by DLS, as the DLS characterizes the CNs with the core and expanded micelles in an aqueous solution, while the electron microscopes characterize the CNs in a dry state. Figure 2F shows the EDS spectra of the as-prepared CNs, indicating that the nanomaterial is composed of 88.24% C and 11.76% O.

The electrochemical performance of CNs/GCE

The characterization of the bare GCE and CNs/GCE has been carried out using cyclic voltammetry (CV) and electrochemical impedance spectroscopy (EIS). The well-defined reversible redox peaks were observed on both bare GCE and CNs/GCE, while the peak current increased significantly after modification of the CNs due to the increase of electroactive surface area (Figure 3A). The electroactive surface area of CNs/GCE was calculated to investigate the electrochemical behavior of the sensing system. The CV was performed with different scan rates from 20 to 100 mV/s in 5.0 mM $[Fe(CN)_6]^{3-/4-}$ solution (Figure 3B). The redox peak current (I_p) followed the linear equation: I_{pa} (μA) = $0.2868 + 9.471\nu^{1/2}$ $(mV/s)^{1/2}$, $R^2 = 0.9983$ and I_{pc} (μA) =

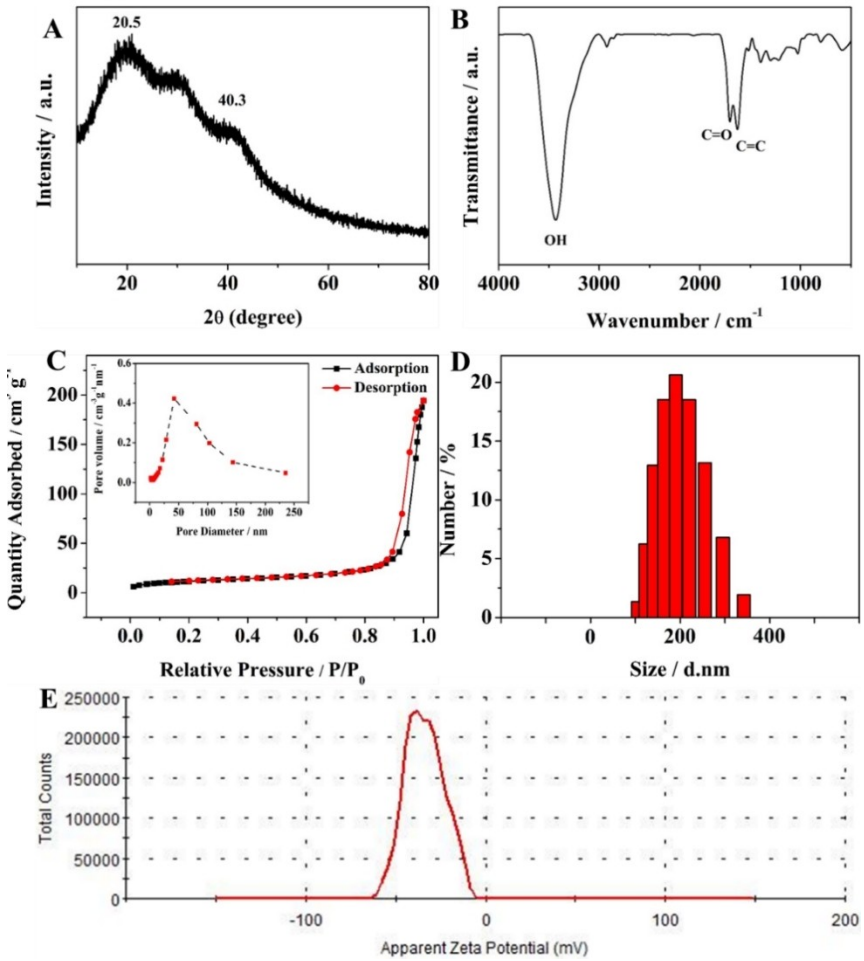

Figure 1. Characterization of the CNs. (A) XRD pattern, (B) FTIR spectra, (C) N_2 adsorption – desorption isotherms, corresponding pore size distribution, (D) DLS, and (E) zeta potential of the CNs.

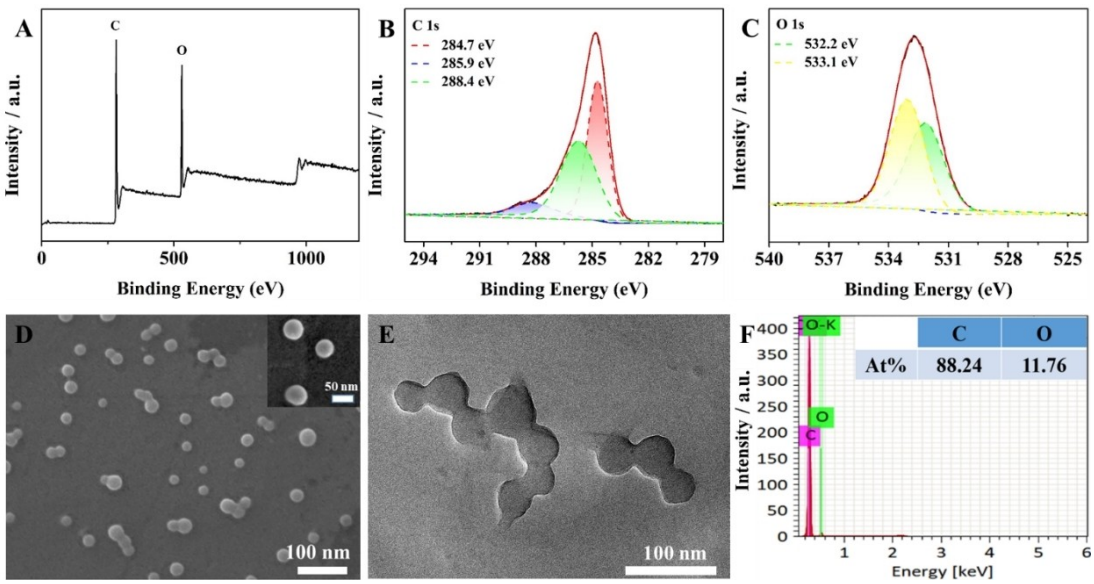

Figure 2. XPS survey (A), C 1s (B) and O 1s (C) spectra of the CNs. FESEM (D) and TEM (E) images of the CNs, insets show the high-magnification images; (F) EDS analysis of the CNs.

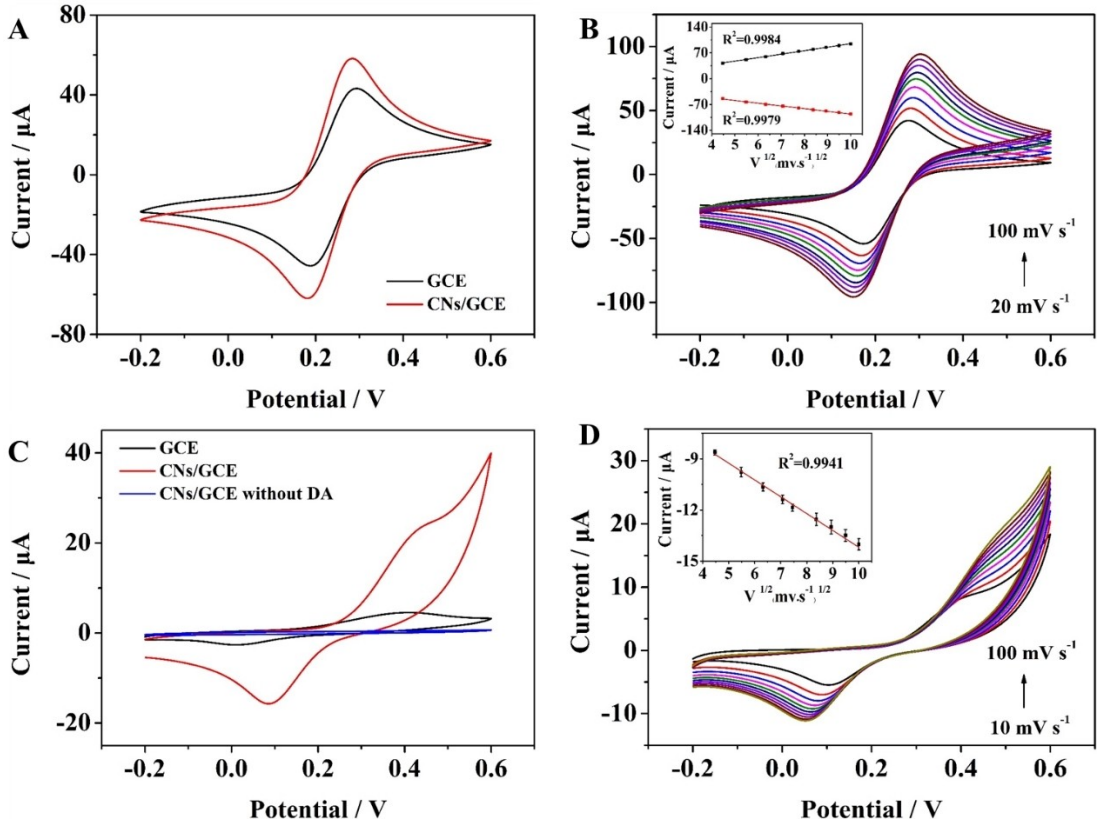

Figure 3. (A) CVs of bare GCE and CNs/GCE in 0.1 M KCl solution containing 5.0 mM $[Fe(CN)_6]^{3-/4-}$; (B) CVs of CNs/GCE with different scan rates 0.1 M KCl solution containing 5.0 mM $[Fe(CN)_6]^{3-/4-}$ (inset: variation of the peak currents with the square root of scan rate); (C) CVs of bare GCE and CNs/GCE in 0.01 M PBS (pH 7.0) containing 0.1 mM DA, and CVs of CNs/GCE without 0.1 mM DA; (D) CVs of CNs/GCE in 0.01 M PBS (pH 7.0) containing 0.1 mM DA at various scan rates 10–100 mV s^{-1} (inset: variation of cathodic peak current (I_{pc}) with the square root of scan rate).

$-22.35-7.374\nu^{1/2}$ $(mV/s)^{1/2}$, $R^2=0.9979$, indicating that the electrochemical process was controlled by diffusion.[24] The electroactive surface area was calculated through the Randles–Sevcik equation:[25]

$$I_p = 268600n^{3/2}AD^{1/2}C\nu^{1/2} \quad (1)$$

in which I_p (A) represents peak current; n (n = 1) represents the number of electron transfers for the $[Fe(CN)_6]^{3-/4-}$ redox reaction; A (cm^2) represents the electroactive surface area; D ($cm^2\,s^{-1}$) and C ($mol\,cm^{-3}$) represent the diffusion coefficient and the concentration of $[Fe(CN)_6]^{3-/4-}$, respectively. ν ($V\,s^{-1}$) represents the scan rate. Herein, n = 1, $D=0.67\times10^{-5}\,cm^2\,s^{-1}$ and $C=5\times10^{-6}\,mol\,cm^{-3}$, thus the average electroactive surface area of the CNs/GCE was calculated to be 0.0349 cm^2. As shown in Figure S2B, the charge transfer resistance (R_{ct}) of the CNs/GCE decreases significantly as compared with the bare GCE, which indicated the facile electron transfer kinetics of the CNs. Figure 3C compares the CV responses to 0.1 mM DA at the bare GCE (black curve) and CNs/GCE (red curve). It can be observed that the oxidation and reduction peak currents obtained at the CNs/GCE were much higher than those obtained at the bare GCE, which can be attributed to the high electroactive area of CNs. In addition, the modification of CNs enabled the increase of reduction peak potential from 0.0 V to 0.1 V due to their electrocatalytic activity. The CV of the CNs/GCE in the absence of DA (blue curve) indicated that no peak current was observed. These results provided strong evidence for the enhanced electrochemical performance of the CNs for DA detection. Figure 3D shows the CVs of DA on the CNs/GCE at different scan rates, the linear regression equation is I_{pc} $(\mu A)=-0.9863\nu^{1/2}$ $(mV/s)^{1/2}-4.324$, $R^2=0.9941$. It is found that the reduction peak current was proportional to the square root of the scan rate, indicating that the electrochemical process was controlled by diffusion.

Effects of amount of CNs and pH on the electrochemical behavior of DA

To maximize the performance of CNs/GCE towards DA determination, the amount of the CNs coated on the GCE was optimized. As shown in Figure 4A, the current response increases with increasing the volume of the CNs from 6–10 μL, and then decreases with further increase of the CNs volume. The change of the current response can be associated with the change in the effective electrode surface area, thus the current initially increased with increasing CN volume. However, further increase in the CNs volume resulted in a thick modification layer at the electrode surface, which may block the electron transfer

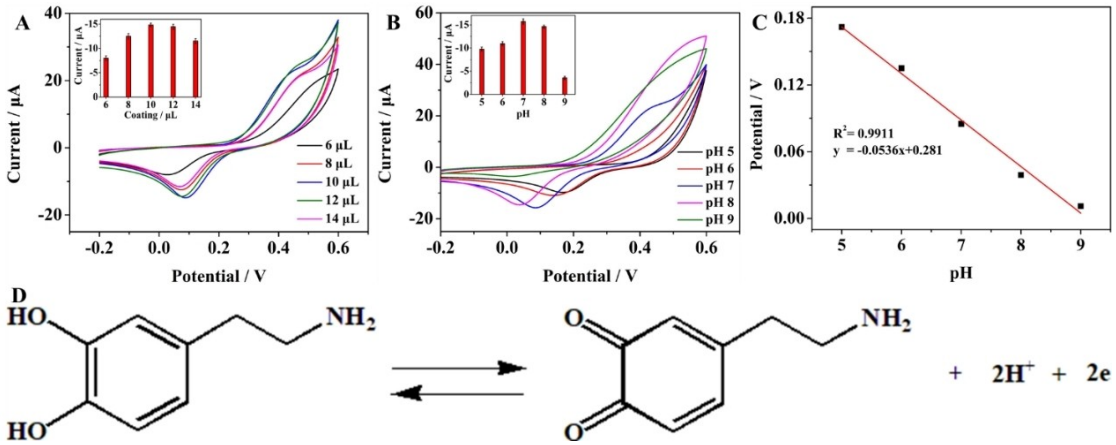

Figure 4. Effect of the amount of CNs (A) and the pH values (B) on the peak currents of 0.1 mM DA at the CNs/GCE; (C) The value of reduction potential of DA versus pH; (D) Mechanistic pathway for the electrochemical reaction of DA.

process. Therefore, 10 μL was chosen for the electrode modification in the following measurements. The pH value of the supporting electrolyte solution directly affects the sensitivity of CNs/GCE for the detection of DA.[26] Figure 4B shows the CV response of the CNs/GCE to 0.1 mM DA in 0.01 M PBS with the pH ranging from 5.0 to 9.0. The results indicate that the peak current increased rapidly as the pH increased, reaching a plateau at pH 7.0, which was selected as the optimal pH for the determination of DA. Figure 4C shows that the reduction potential of DA is linear to the pH value ranging from 5.0 to 9.0, with the linear regression equation of E_p (V) = −0.0536pH + 0.281 (R^2 = 0.9911). The attained slope was close to −0.059, indicating that the electrochemical oxidization reaction on the CNs/GCE was a two − electron transfer process for DA.[27–29] The reaction mechanism was shown in Figure 4D.

Differential pulse voltammetric detection of DA

DPV was employed to detect DA on the CNs/GCE by investigation of the current responses to different concentrations of DA (0.05 to 1600 μM) in 0.01 M PBS (pH 7.0). As shown in Figure 5A, the CNs/GCE exhibit strong current response to the increase of the DA concentration. Figure 5B indicates that the peak currents are linear with the concentrations of DA, with regression equations I_{pc}(μA) = −0.0754 C(μM) − 3.02, R^2 = 0.9947 for the low DA concentration region (0.05–150 μM) and I_{pc}(μA) = −0.0226 C(μM) − 13.03, R^2 = 0.9958 for the DA concentration range of 150–1600 μM. The limit of detection was determined to be 8.3 nM using the first linear segment based on $3S_b/k$, where S_b is the standard deviation of the blank solution and k is the slope of the regression. Table 1 compares the analytical performance of the CNs/GCE with that of the electrochemical sensors reported previously for DA detection. Obviously, the detection limit of DA achieved at the CNs/GCE was among the lowest. Meanwhile, its linearity for DA determination ranged from 0.05 to 1600 μM, which was wider than that obtained with other modified electrodes (Table 1). It is noteworthy that most of these modified electrodes were prepared by metal and/or metal oxide materials such as Au and TiO_2, however, the CNs/GCE proposed in this work achieved better performance by using a cheap material with a simple synthetic route, which is

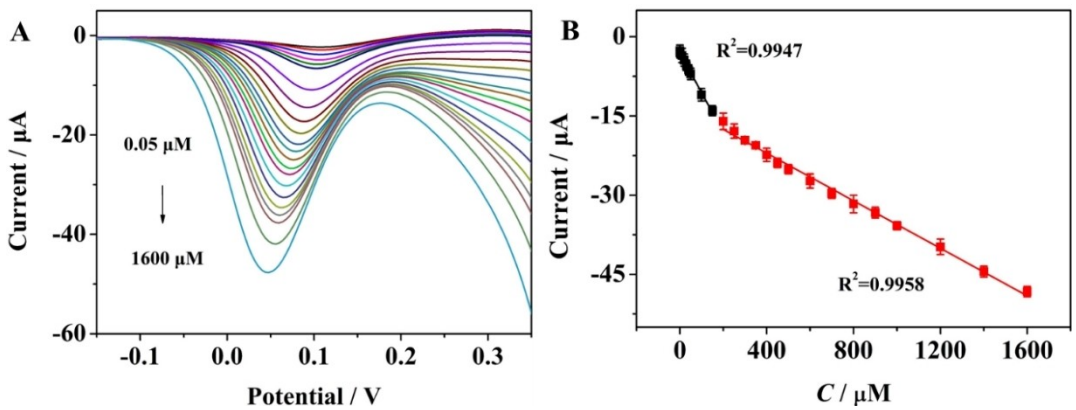

Figure 5. (A) DPV curves of the CNs/GCE with the variation of the DA concentrations from 0.05 to 1600 μM; (B) Calibration curves of DPV peak currents versus the concentrations of DA from 0.05 to1600 μM at the CNs/GCE.

Table 1. The analytical performance of electrochemical sensors for DA detection.

Electrode	Method	Linear range [μM]	Detection limit [μM]	Ref.
Fe_3O_4/SnO_2/Gr/CPE	DPV	0.02–2.8	0.0071	[30]
Cu/Cu_2O–OA/MWCNTs/GC	DPV	0.02–0.159	0.00327	[31]
L–cys ZnS:Mn QDs	Phosphorescence	0.15–3.00	0.0078	[32]
G-30	DPV	3–140	1.44	[33]
β–CD@AuNCs	Fluorescence	0.1–80	0.02	[34]
rGO/Co_3O_4/GCE	CA	0–30	0.277	[35]
Ti_3C_2–MXene–FET	DPV	0.1–50	0.1	[36]
HNP–PtTi	DPV	4–500	3.2	[37]
GQDs/IL–SPCE	DPV	0.2–15	0.06	[38]
TiO_2 microtube	DPV	0.4–80	0.025	[39]
NACP film electrode	DPV	0.05–15	0.01	[40]
CNs/GCE	DPV	0.05–1600	0.0083	This work

highly desirable for the development of cost-effective and high-performance sensing devices.

Selectivity, reproducibility, repeatability, and stability of CNs/GCE

Selectivity is an important parameter for the evaluation of the applicability of CNs/GCE for DA sensing, as some electroactive substances that usually exist in human body fluids can affect the electrochemical detection of DA. Figure 6A demonstrates that none of the common interferents produced a notable current response on the CNs/GCE as compared with DA, which is satisfactory for selective detection of DA. The reproducibility of CNs/GCE was assessed by using six independent CNs/GCEs under identical fabrication and measurement conditions for DA detection. As shown in Figure 6B, the relative standard deviation (RSD) of intraday reproducibility was 4.1 %, which indicates the good reproducibility of the proposed CNs/GCE. The repeatability of CNs/GCE was tested for 20 times in 0.01 M PBS

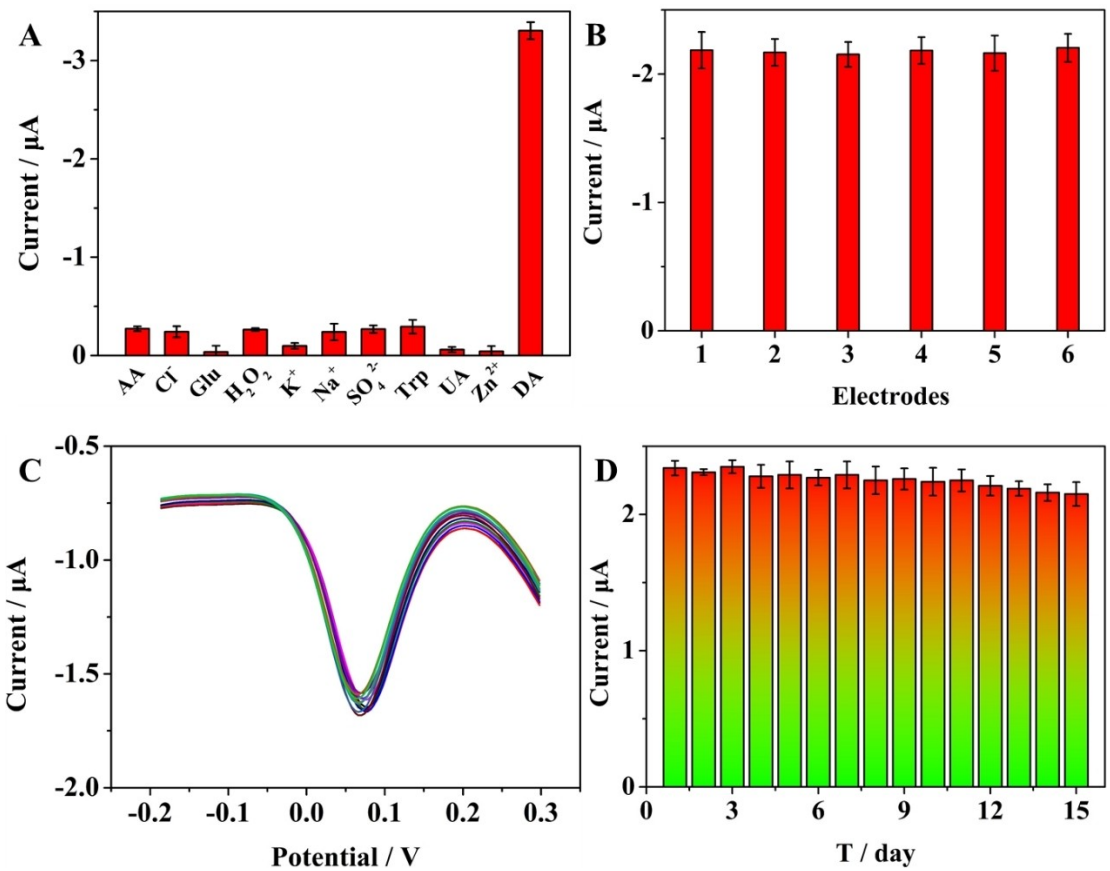

Figure 6. (A) The selectivity of CNs/GCE for the detection of 20 μM DA in the presence of 10-fold excess of different interferents (K^+, Na^+, Zn^{2+},Cl^-, SO_4^{2-}, AA, UA, Glu, H_2O_2, Trp); (B) The reproducibility of CNs/GCE for the detection of 20 μM DA at 6 different electrodes; (C) The repeatability of the same CNs/GCE for 20 consecutive measurements of 20 μM DA; (D) The stability of CNs/GCE for measuring DA responses over 15 days.

containing 20 μM DA, and results are presented in Figure 6C. The current response retained 89.87% of the original value after 20 times of continuous measurement. Moreover, the stability of the CNs/GCE was evaluated by measuring the current response in 20 μM DA on a daily basis for 15 days. The CNs/GCE displayed a relatively stable performance for repeated measurements, showing a 97.2% retention of the initial response. The response decreased to 89.6% upon consecutive scans after 15 days (Figure 6D). The original DPV curves of stability and reproducibility were shown in Figure S4. Overall, The CNs/GCE displayed good selectivity, reproducibility, repeatability, and stability, which are attractive for the development of effective DA sensors in practical applications.

Spiked serum sample studies

To demonstrate the potential of CNs/GCE in clinical applications, its responses to spiked DA in serum samples at different concentrations (5 μM, 100 μM and 500 μM) were measured. The average recoveries varied from 99.71% to 105.60% with relative standard deviations (RSD) less than 3.57% (Table S1). The satisfactory results suggest that the CNs/GCE can be effectively applied for the analysis of real samples.

Conclusion

The CNs, synthesized through a simple and green hydrothermal method, were found to exhibit high electrocatalytic activities for the determination of DA with a wide linear range, low LOD, good stability, excellent selectivity, and reproducibility. The CNs/GCE was employed for the analysis of different concentrations of DA in human blood serum samples, which obtained satisfactory recoveries ranging from 99.71% to 105.60%. The proposed strategy provides a facile route to the design of electrochemical sensors with high performance and low cost, as well as future capabilities of mass production for a variety of sensing applications.

Experimental Section

Materials and reagents

Glucose, dopamine (DA), epinephrine (EP), ascorbic acid (AA), uric acid (UA), glutathione (GSH), tryptophan (Trp), hydrogen peroxide (H_2O_2) were purchased from Aladdin Chemistry Co., Ltd. (Shanghai, China). All solutions were prepared with ultrapure water (resistivity: 18.25 MΩ cm).

Preparation of the CNs and CNs/GCE

In a typical preparation procedure, 5.0 g glucose was dissolved in 80 mL ultrapure water and sonicated for 60 min. Then, the obtained solution was transferred into a 100 mL autoclave, and the hydrothermal reaction was executed at 180 °C for 6 h. The puce products were separated by centrifugation at 10000 rpm for 15 min and washed with ethanol and deionized water for 4 times. Then, the solution was dialyzed with ultrapure water for 24 h to produce uniformly sized CNs. The CNs were harvested by freeze-drying the aforesaid solutions. Before each electrochemical test, a glassy carbon electrode (GCE) was polished with 0.05 μm alumina slurry and then cleaned ultrasonically in ultrapure water and ethanol to give a clean surface. The as-synthesized CNs were dispersed in ultrapure water (2 mg mL^{-1}), which was modified onto the cleaned GCE by drop casting, followed by vacuum drying to produce the CNs/GCE biosensor.

Acknowledgements

The research was financially supported by National Natural Science Foundation of China (No. 21874087 and 22274090), Shanxi Scholarship Council of China (2021-012) and James Cook University.

Conflict of Interest

The authors declare no conflict of interest.

Data Availability Statement

The data that support the findings of this study are available from the corresponding author upon reasonable request.

Keywords: Carbon nanospheres · Dopamine detection · Green synthesis · Human serum samples

[1] H. Li, K. Zhou, J. Cao, Q. Wei, C. Lin, S. E. Pei, L. Ma, N. Hu, Y. Guo, Z. Deng, Z. Yu, S. Zeng, W. Yang, L. Meng, *Carbon* **2021**, *171*, 16–28.
[2] T. Subramaniam, G. Kesavan, G. Venkatachalam, *ACS Appl. Bio Mater.* **2020**, *3*, 7769–7778.
[3] Z. Qu, Y. Muhammad, W. He, J. Li, Z. Gao, J. Fu, S. J. Shah, H. Sun, J. Wang, Z. Huang, Z. Zhao, *Chem. Eng. J.* **2021**, *404*, 126570.
[4] Y. C. Jia, Z. Cheng, G. H. Wang, S. M. Shuang, Y. H. Zhou, C. Dong, F. F. Du, *Food Chem.* **2023**, *40*, 134245.
[5] J. F. van Staden, R. I. S. van Staden, *Talanta* **2012**, *102*, 34–43.
[6] C. Zhao, Y. Jiao, J. Hua, J. Yang, Y. Yang, *J. Fluoresc.* **2018**, *28*, 269–276.
[7] X. Li, J. Pan, F. Yang, J. Feng, J. Mo, Z. Chen, *Microchim. Acta* **2011**, *174*, 123–130.
[8] W. He, R. Liu, P. Zhou, Q. Liu, T. Cui, *Biosens. Bioelectron.* **2020**, *167*, 112473.
[9] Z. Lu, Y. Li, T. Liu, G. Wang, M. Sun, Y. Jiang, H. He, Y. Wang, P. Zou, X. Wang, Q. Zhao, H. Rao, *Chem. Eng. J.* **2020**, *389*, 124417.
[10] W. Liu, F. Cui, H. Li, S. Wang, B. Zhuo, S. Wang, *Sens. Actuators B* **2020**, *323*, 128669.
[11] P. Lei, Y. Zhou, G. Zhang, Y. Zhang, C. Zhang, S. Hong, Y. Yang, C. Dong, S. Shuang, *Talanta* **2019**, *195*, 306–312.
[12] P. Lei, Y. Zhou, R. Zhu, Y. Liu, C. Dong, S. Shuang, *Biosens. Bioelectron.* **2020**, *147*, 111735.
[13] J. Xiong, Q. Bian, S. Lei, Y. Deng, K. Zhao, S. Sun, Q. Fu, Y. Xiao, B. Cheng, *Nanoscale* **2021**, *13*, 5369–5382.
[14] Y. Hashikawa, T. Fushino, Y. Murata, *J. Am. Chem. Soc.* **2020**, *49*, 20572–20576.
[15] C. Tsai, H. Tai, C. Su, L. Chiang, Y. Li, *ACS Appl. Nano Mater.* **2020**, *3*, 10380–10388.
[16] H. Zhang, T. Wu, Y. Chen, Q. Zhang, Z. Chen, Y. Ling, Y. Jia, Y. Yang, X. Liu, Y. Zhou, *Nanoscale* **2021**, *13*, 10943–10952.
[17] N. Li, Y. Guan, Y. Li, H. Mi, L. Deng, L. Sun, Q. Zhang, C. He, X. Ren, *J. Mater. Chem. A* **2021**, *9*, 1143–1149.

[18] X. Liu, M. M. Vadiyar, J. Kwon Oh, Z. Ye, *ACS Appl. Mater. Interfaces* **2021**, *13*, 32916–32929.
[19] J. Xi, C. Xie, Y. Zhang, L. Wang, J. Xiao, X. Duan, J. Ren, F. Xiao, S. Wang, *ACS Appl. Mater. Interfaces* **2016**, *8*, 22563–22573.
[20] J. Yan, H. Duan, L. Miao, L. Ruhlmann, Y. Lv, W. Xiong, D. Zhu, L. Li, L. Gan, M. Liu, *Electrochim. Acta* **2020**, *358*, 136899–136908.
[21] X. Wen, D. Zhang, L. Shi, T. Yan, H. Wang, J. Zhang, *J. Mater. Chem.* **2012**, *22*, 23835–23844.
[22] B. R. Selvi, D. Jagadeesan, B. S. Suma, G. Nagashankar, M. Arif, K. Balasubramanyam, M. Eswaramoorthy, T. K. Kundu, *Nano Lett.* **2008**, *8*, 10.
[23] P. Lei, Y. Zhou, R. Zhu, C. Dong, S. Wu, S. Shuang, *Sens. Actuators B* **2021**, *326*, 128863.
[24] Y. Liu, L. Zhang, N. Zhao, Y. Han, F. Zhao, Z. Peng, Y. Li, *Analyst* **2017**, *142*, 1091–1098.
[25] B. B. Prasad, A. Kumar, R. Singh, *Biosens. Bioelectron.* **2017**, *94*, 1–9.
[26] J. Huang, Y. Liu, H. Hou, T. You, *Biosens. Bioelectron.* **2008**, *24*, 632–637.
[27] J. Wang, B. Yang, J. Zhong, B. Yan, K. Zhang, C. Zhai, Y. Shiraishi, Y. Du, P. Yang, *J. Colloid Interface Sci.* **2017**, *497*, 172–180.
[28] Z. Xu, F. Liu, T. Zhang, Y. Gu, N. Lu, H. Xu, X. Yan, Y. Song, Y. Xing, D. Yu, Z. Zhang, P. Lu, *Anal. Chem.* **2020**, *92*, 15297–15305.
[29] Y. Dong, J. Zheng, *Sens. Actuators B* **2020**, *311*, 127918.
[30] H. Bagheri, N. Pajooheshpour, B. Jamali, S. Amidi, A. Hajian, H. Khoshsafar, *Microchem. J.* **2017**, *131*, 120–129.
[31] M. Devaraj, R. Saravanan, R. Deivasigamani, V. K. Gupta, F. Gracia, S. Jayadevan, *J. Mol. Liq.* **2016**, *221*, 930–941.
[32] D. Diaz-Diestra, B. Thapa, J. Beltran-Huarac, B. R. Weiner, G. Morell, *Biosens. Bioelectron.* **2017**, *87*, 693–700.
[33] L. Fu, A. Wang, G. Lai, W. Su, F. Malherbe, J. Yu, C. Lin, A. Yu, *Talanta* **2018**, *180*, 248–253.
[34] M. I. Halawa, F. Wu, T. H. Fereja, B. Lou, G. Xu, *Sens. Actuators B* **2018**, *254*, 1017–1024.
[35] A. Numan, M. M. Shahid, F. S. Omar, K. Ramesh, S. Ramesh, *Sens. Actuators B* **2017**, *238*, 1043–1051.
[36] B. Xu, M. Zhu, W. Zhang, X. Zhen, Z. Pei, Q. Xue, C. Zhi, P. Shi, *Adv. Mater.* **2016**, *28*, 3333–3339.
[37] D. Zhao, G. Yu, K. Tian, C. Xu, *Biosens. Bioelectron.* **2016**, *82*, 119–126.
[38] K. Kunpatee, S. Traipop, O. Chailapakul, S. Chuanuwatanakul, *Sens. Actuators B* **2020**, *314*, 128059.
[39] F. Ma, B. Yang, Z. Zhao, Y. Zhao, R. Pan, D. Wang, Y. Kong, Y. Chen, G. Huang, J. Kong, Y. Mei, *ACS Appl. Nano Mater.* **2020**, *3*, 10032–10039.
[40] Y. Shu, Q. Lu, F. Yuan, Q. Tao, D. Jin, H. Yao, Q. Xu, X. Hu, *ACS Appl. Mater. Interfaces* **2020**, *12*, 49480–49488.

Manuscript received: December 1, 2022
Revised manuscript received: January 1, 2023